Title
Versatility of the CFR Algorithm for Limited Angle Reconstruction

Authors
Fujieda, I.
Heiskanen, K.
Perez-Mendez, V.

Publication Date
1989-08-01

Lawrence Berkeley Laboratory
UNIVERSITY OF CALIFORNIA

Physics Division

Presented at the IEEE Nuclear Science Symposium,
San Francisco, CA, October 25–27, 1989, and
to be published in IEEE Transactions on Nuclear Science

Versatility of the CFR Algorithm for Limited Angle Reconstruction

I. Fujieda, K. Heiskanen, and V. Perez-Mendez

August 1989

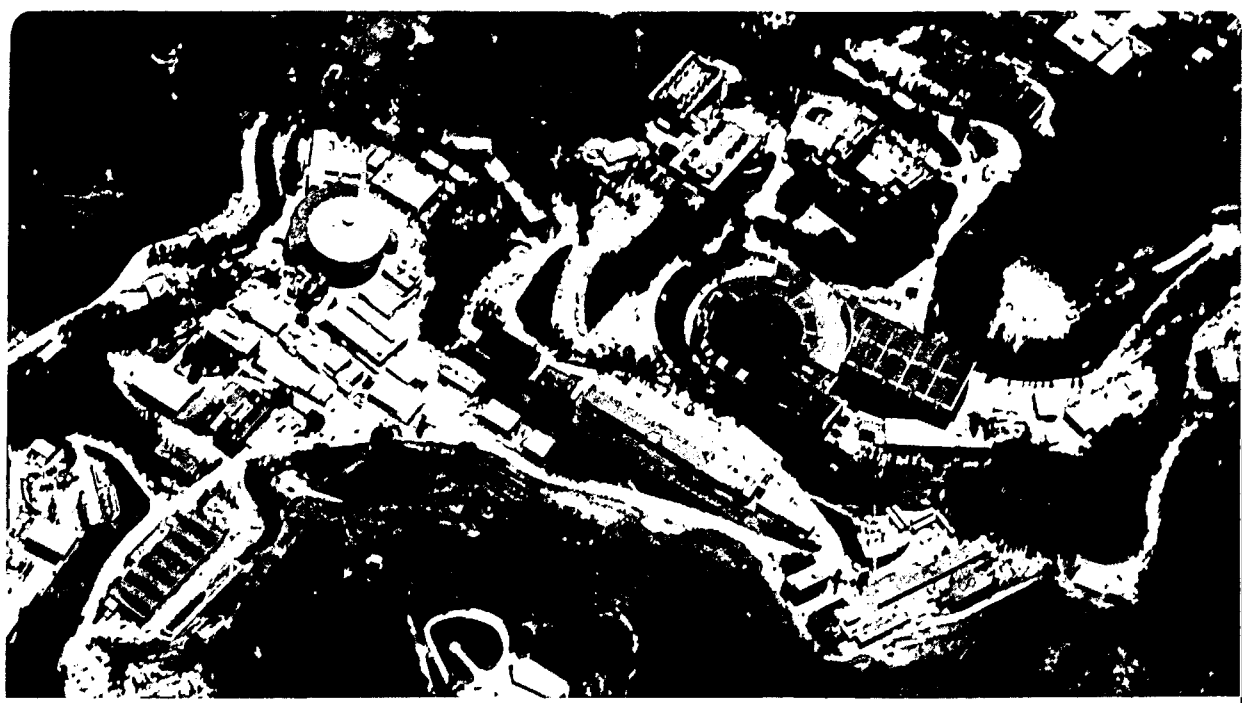

Prepared for the U.S. Department of Energy under Contract Number DE-AC03-76SF00098.

DISCLAIMER

VERSATILITY OF THE CFR ALGORITHM FOR LIMITED ANGLE RECONSTRUCTION

I. Fujieda, K. Heiskanen and V. Perez-Mendez

Abstract

The Constrained Fourier Reconstruction (CFR) algorithm and the Iterative Reconstruction-Reprojection (IRR) algorithm are evaluated based on their accuracy for three types of limited angle reconstruction problems. The CFR algorithm performs better for problems such as Xray CT imaging of a nuclear reactor core with one large data gap due to structural blocking of the source and detector pair. For gated heart imaging by Xray CT, radioisotope distribution imaging by PET or SPECT, using a polygonal array of gamma cameras with insensitive gaps between camera boundaries, the IRR algorithm has a slight advantage over the CFR algorithm but the difference is not significant.

I. INTRODUCTION

A limited angle reconstruction problem arises whenever a complete set of projection data are not available for various reasons. Reconstruction without special consideration of the missing projection data often causes severe artifacts. This problem has been treated by many authors and to our knowledge, the most recent discussion and comparison of some algorithms are given by Ollinger and Karp[1]. They evaluated three algorithms (ISRA, PSIRR, CFR) for their incomplete projection data obtained by their PENN-PET which has six 5^{o} insensitive gaps in the hexagonal array of gamma camera. They concluded that the computational advantage of the CFR algorithm outweighed its slight disadvantage in accuracy. While this is true for the PENN-PET type incomplete projection data, it is useful to know how these algorithms perform for different types of limited angle reconstruction problems. We have chosen to compare two transform algorithms i.e. the CFR and the IRR due to their relatively light computational burden and simple implementation. Both algorithms enable us to use the filtered back-projection (FBP), the efficient and predominant reconstruction algorithm for computed tomography (CT). We consider here three types of limited angle reconstruction problems and evaluate these two algorithms based on their accuracy. Since both consist of an iteration process, the error is defined and calculated after each iteration to check their convergence. In the following sections, three types of limited angle reconstruction problems are described, the CFR and the IRR algorithms are reviewed. Images reconstructed by these two algorithms from simulated incomplete projection data are shown.

This work was supported by the Director, Office of Energy Research, Office of High Energy and Nuclear Physics, division of High energy Physics of the U.S. Department of Energy under contract No. DE-AC03-76SF00098.

The authors are with Lawrence Berkeley Laboratory, 1 Cyclotron Rd., Berkeley, CA 94720.

II. THREE TYPES OF LIMITED ANGLE RECONSTRUCTION PROBLEMS

Figure 1 shows three types of situations where limited angle reconstruction problems arise.

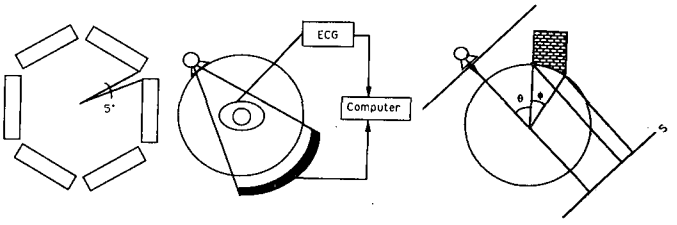

Fig.1 Three types of limited angle reconstruction problems. (a) PENN-PET case, (b) gated heart imaging and (c) gap angle geometry.

The first one is the PENN-PET case already discussed by Ollinger and Karp[1] (Fig.1(a)). The small insensitive gaps in the stationary hexagonal array of gamma cameras result in incomplete data acquisition. Multicrystal PET and SPECT systems with malfunctioning detectors also fall in this category because one dead detector is equivalent to one small insensitive gap in the detector array. This PENN-PET case is included to verify that we can reproduce the results of Ollinger and Karp; it is also meant as a double-check of our implementation of the reconstruction algorithms.

The second type considered here is the case of gated cardiac imaging using Xray CT (Fig.1(b)). Each stage of the heart motion is to be imaged by a finite number of Xray source-detector pair rotations which are limited by the breath-holding time. Each stage of the heart motion is identified by separately monitored ECG signal. Since the ECG signal is not synchronized with the source-detector pair rotation, projections through the heart for all angles between 0^{o} and 360^{o} are not available within a finite data collection time for each stage of the heart motion.

The third type of limited angle reconstruction problems is the case where one large data gap exists due to structural blocking around the object to be imaged (fig.1(c)). Imaging a nuclear reactor core by Xray CT as well as coronal or sagital imaging of the human body by PET, SPECT or Xray CT are examples of this type. We term this situation "gap angle geometry."

III. ALGORITHM REVIEW AND EVALUATION METHOD

Figure 2 shows the flow charts for the two algorithms used in this study, namely, the CFR (constrained Fourier

Reconstruction)[2] and the IRR (Iterative Reconstruction-Reprojection). The projection data are expressed as $p_o(s,\theta)$ where s and θ are the usual coordinates for the sinogram representation, i.e. θ is the angle of a projection line and s is the coordinate perpendicular to the projection line. In Fig.2, both algorithms start from the original incomplete projection data $p_o(s,\theta)$. In the first iteration, $p_i(s,\theta)=p_o(s,\theta)$. The CFR algorithm performs two-dimensional Fourier Transform (2D-FT) on $p_i(s,\theta)$ with respect to s and θ. The resultant Fourier coefficients $P(\omega,n)$ are masked by $H(\omega,n)$ which retains Fourier coefficients satisfying the relation,

$$|n| < R_{obj}|\omega| \tag{1}$$

where R_{obj} is the object radius. Inverse Fourier Transform of

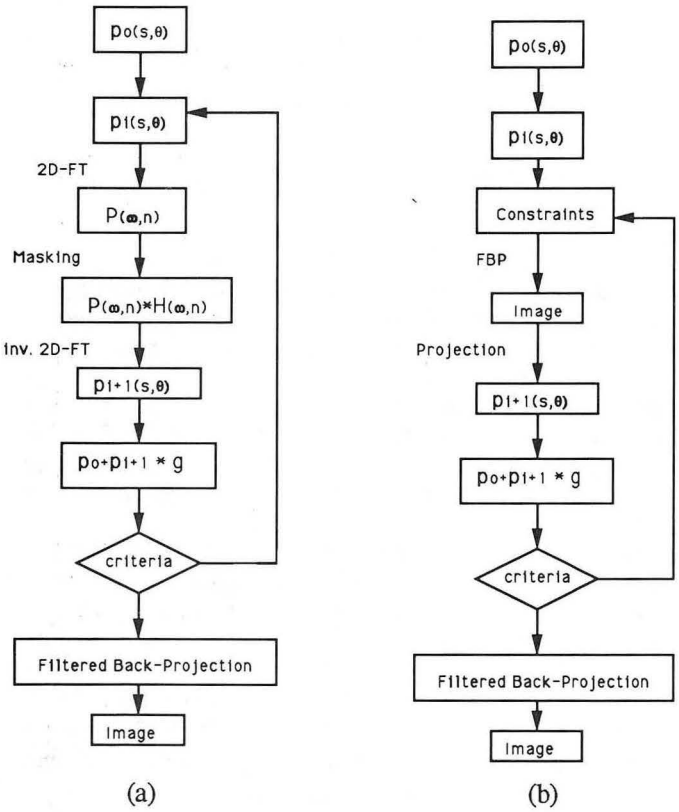

Fig.2 Flow charts of (a) the CFR algorithm and (b) the IRR algorithm.

the masked Fourier coefficients gives $p_{i+1}(s,\theta)$, the new estimate of the projection data which include the missing gap data. These gap data created by the process mentioned above are extracted from $p_{i+1}(s,\theta)$ by multiplying the factor $g(s,\theta)$, where $g(s,\theta)=1$ for the missing data and $g(s,\theta)=0$ otherwise. The original data $p_o(s,\theta)$ is added to the extracted gap data to give the (i+1)th estimate of the projection data. This new estimate is used for the input and the iteration continues until it satisfies some criteria. An image is reconstructed by the filtered back-projection (FBP) using the resultant projection data.

The IRR applies constraints directly on the sinogram. The constraints are based on the a-priori knowledge about the object size, non-negativity and the upper limit of pixel values. Filtered back-projection (FBP) and reprojection process create the data missing in $p_o(s,\theta)$. They are extracted and added to $p_o(s,\theta)$ to give the next estimate of the projection data. This is used as the input for the next iteration. Finally, the image is reconstructed by the FBP after some criteria are met.

In order to evaluate how the iteration improves a simulated incomplete sinogram, an error index is defined as the "distance" between the ith estimate of the projection data $p_i(s,\theta)$ and the known projection data $p^*(s,\theta)$ by the following equation.

$$d = \sqrt{\sum_{s,\theta} (p_i(s,\theta) - p^*(s,\theta))^2} \tag{2}$$

IV. SIMULATION

The CFR and the IRR are implemented in the VAX environment using the standard set of reconstruction softwares developed by Huesman et al.[3]. A simple phantom which contains two low pixel value areas ("lungs") and one high pixel value area ("bone" or "heart") is assumed for all the three cases shown in Fig.1. The size of the image is 64X64 pixels. Parallel data collection is assumed for simplicity.

The extent to which the gap in the detector array affects the data collection is best illustrated by the case of Fig.1(c). Since the detector-source pair cannot move through the blocking object, projection lines that satisfy the relation,

$$R_0 \sin\theta < s < R_0 \sin(\theta+\phi) \tag{3}$$

cannot be observed. R_o is the radius of the field of view, ϕ is the gap angle as shown in Fig.1(c). This creates a sinusoidal pattern in a sinogram as shown in Fig.3(c). The width of the

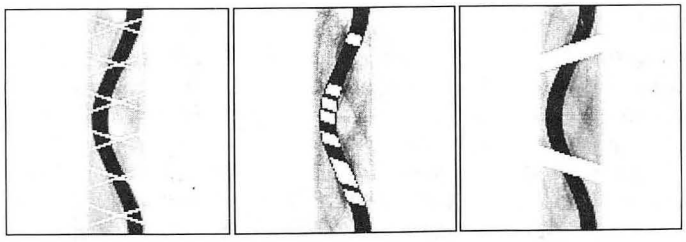

(a) (b) (c)

Fig.3 Sinogram representation of the simulated projection data for the three types of problems: (a) PENN-PET case, (b) gated heart imaging and (c) gap angle geometry.

sinusoidal pattern in θ direction is equal to ϕ. Fig.3(c) shows the case of $\phi=30^o$. The range of θ is $0^o<\theta<360^o$.

The PENN-PET case shown in Fig.1(a) has six 5^o gaps, therefor its sinogram has six sinusoidal patterns of 5^o width in

θ direction with 60° separation between each other. This creates a cross pattern as shown in Fig.3(a).

The case of gated hart imaging needs a little more attention in creating the incomplete sinogram. The ECG cycle is divided into 20 equal durations during which the heart is assumed stationary. The heart beat rate is about 60/min, so that this duration becomes about 50msec. It takes a few seconds for the source-detector pair to rotate around the body. It keeps on rotating and collecting data as long as the patient holds his breath. Due to the fan-beam data collection, the projection lines are filled in the sinogram of the usual (s,θ) coordinate system along the curves,

$$s = R_0 \sin(\theta+\beta), \quad |\beta| < \frac{\beta_d}{2} \qquad (4)$$

where R_0 and β_d are the radius of the field of view and the angle opening of the fan-beam, respectively. During the first rotation, only a few values of θ around which the projection data are filled are available for each stage of the heart motion. Next rotation gives a few more of these projection data which may or may not overlap the data obtained by the first rotation, depending on the synchronization between the heart motion and the source-detector pair rotation. After 10 to 20 rotations which correspond to the breath-holding time, we obtain 20 sinograms, each corresponding to one heart motion stage. Fig.3(b) shows one of these sinograms. Only the projection lines through the heart at certain angular ranges along the curves eq.(4) are missing because the other parts of the body are projected 10 to 20 times and those projection lines are available. About 40% of the data originating from the heart are missing in Fig.3(b) and this missing fraction is a reasonable estimate based on the 30sec data collection time (breath-holding time) and a few seconds rotation time for a typical Xray CT.

V. RESULTS AND DISCUSSIONS

The error index defined by eq.(2) is calculated after each iteration of the CFR and the IRR algorithms for the three incomplete sinograms shown in Fig.3. The results are plotted in Fig.4. For the PENN-PET case (Fig.4(a)), both algorithms show similar convergence, which is consistent with the results by Ollinger and Karp[1]. For the gated heart imaging, the IRR gives a slightly smaller error (Fig.4(b)). For the gap angle geometry with a 30° gap angle, however, the IRR diverges after 4-5 iterations whereas the CFR converges steadily.

The difference of these two algorithms in handling these limited angle reconstruction problems may be understood in the following manner. The CFR algorithm, in principle, is effective for erasing a sinusoidal curve from the sinogram if its amplitude is larger than the object radius. This is the case for Fig.3(a) and (c). Fig3.(a) has six thin sinusoidal patterns superimposed on each other with 60° phase separation. Fig.3(c) has one thick sinusoidal pattern. The amplitude of these sinusoidal curves is equal to the radius of the field of view and is larger than the object radius. The IRR performs the filtered back-projection; filtering an incomplete projection profile introduces a large error especially when the missing fraction is large and concentrated at one region of s coordinate as in the case of Fig.3(c). This explains the superiority of the CFR algorithm for the large gap angle geometry. As for the case of gated heart imaging, there is no clear advantage of the CFR algorithm except for its shorter computation time, because the missing data does not form complete sinusoidal curves.

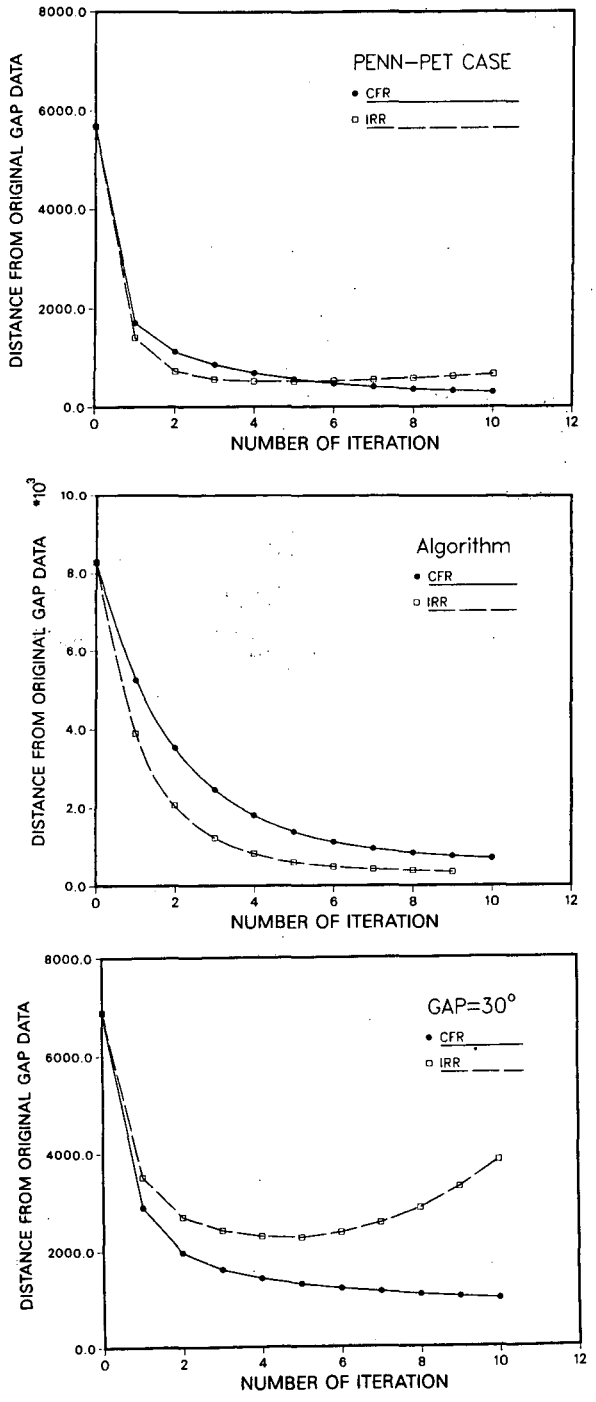

Fig.4 The convergence of the CFR and the IRR algorithms for (a) PENN-PET case, (b) gated heart imaging and (c) gap angle geometry.

Another way to evaluate algorithms is simply to look at the reconstructed images. Figure 5 (a),(b),(c) are the images reconstructed from the incomplete sinograms shown in Fig.3 (a),(b),(c), respectively, without any compensation methods. The results of the CFR algorithm are shown in Fig.5 (d),(e),(f). These are reconstructed after 10 iterations. Now the "lungs" and the "heart" are all visible in all cases. The last row of Fig.5 shows the results of the IRR algorithm after 10 iterations for (g) and (h) and 5 iterations for (i). For Fig.5(i), the iteration is stopped at the point of the minimum error as shown in Fig.4(c). There exists a noticeable artifact in (g) and (i). This strip-shaped artifact becomes pronounced as the iteration proceeds and is related to the divergence of the error index in Fig.4(c). The same trend can be seen in Fig.4(a) to a much lesser extent. This fact suggests that the error induced in the filtering process of the FBP tends to accumulate as the iteration proceeds. This error accumulation has more profound effects for the large gap angle geometry where more data in the projection profiles at a certain angle are missing. In the case of gated heart imaging (Fig.5(h)), there is little error accumulation because only a small amount of the data in a projection profile at a certain angle is missing.

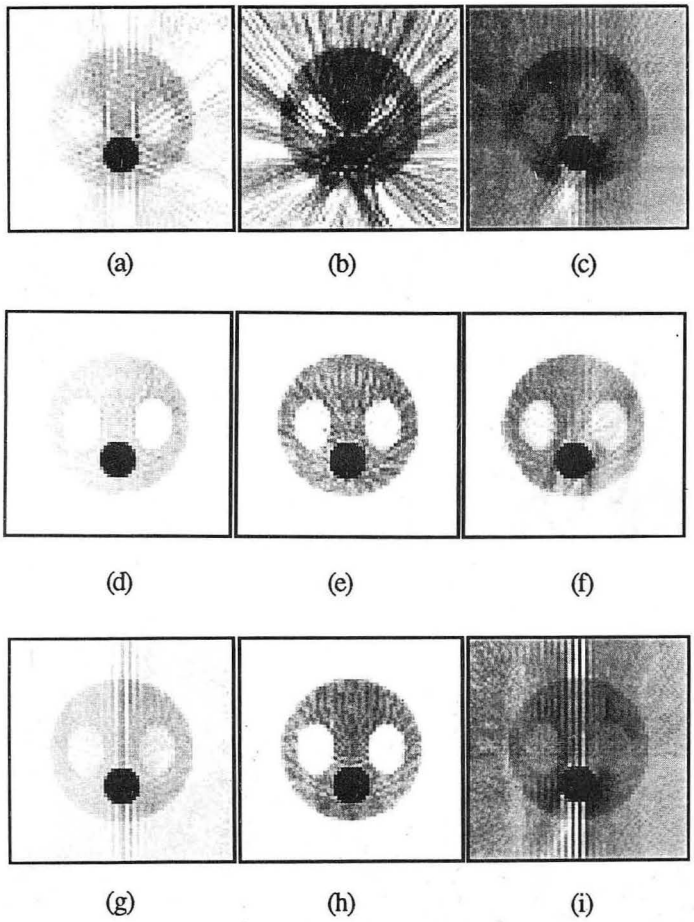

Fig.5 Reconstructed images for the PENN-PET case without compensation (a), by the CFR (d), by the IRR (g), for gated heart imaging without compensation (b), by the CFR (e), by the IRR (h), and for the gap angle geometry without compensation (c), by the CFR (f), by the IRR (i).

VI. CONCLUSION

We have applied the two algorithms (CFR and IRR) for the three types of simulated limited angle reconstruction problems. For the PENN-PET case where small insensitive gaps are distributed over 360^{o}, both algorithms give good estimates of the missing data. The IRR algorithm has a slight tendency to diverge after several iterations and there is a slight but noticeable strip-shaped artifact in the reconstructed image. For the case of gated heart imaging where only the projection lines through the heart in certain angular ranges are missing, both algorithms perform equally well with a slight advantage in accuracy for the IRR. For imaging an object with structural blocking, the CFR performs better, especially when the gap angle is large. The IRR diverges after several iterations and the strip-shaped artifact in the reconstructed image becomes more pronounced. We attribute this difference in performance to the CFR's capability of removing a large sinusoidal pattern from a sinogram and the error accumulation of the filtering process in the IRR.

Overall, the CFR algorithm is versatile and more practical especially for a large gap angle geometry with the additional advantages of less computation time and better convergence.

REFERENCES

[1] J.M.Ollinger and J.S.Karp, IEEE Trans. Nucl. Sci. NS-35(1988)629.

[2] J.S.Karp, G.Muehllener and R.M.Lewitt, IEEE Trans. Medical Imaging, MI-7(1988)21.

[3] R.H.Huesman, G.T.Gullberg, W.L.Greenberg and T.F.Budinger, LBL PUB-214, Oct.1977.

LAWRENCE BERKELEY LABORATORY
TECHNICAL INFORMATION DEPARTMENT
1 CYCLOTRON ROAD
BERKELEY, CALIFORNIA 94720